Analysis of a new Red-Black Ordering for Gauss-Seidel Smoothing in Cell-Centred Multigrid

Article · July 1996

Source: CiteSeer

1 author:

Thor Gjesdal
Forsvarets forskningsinstitutt
16 PUBLICATIONS **152** CITATIONS

SEE PROFILE

Analysis of a new Red-Black Ordering for Gauss-Seidel Smoothing in Cell-Centred Multigrid

Thor Gjesdal *

November, 1993

Abstract

Based on numerical experiments with a cell-centred multigrid Poisson solver in one and two dimensions, we propose to use Alternating Coarse-Line Zebra ordering as a robust parallel smoother for the 2D case. The algorithm is presented based on a heuristic discussion, and the convergence rates obtained with different smoothers are compared. Local mode analysis is used to estimate the smoothing factor and two-level convergence for the method.

1991 Mathematical Subject Classification: 65N22, 65N55, 65Y05

1 Introduction

During the last decade and a half, there has been a steady increase in the interest of using and developing multigrid methods for the numerical solution of partial differential equations. Unlike other iterative methods, multigrid algorithms offer convergence rates that are independent of the number of grid points. This is achieved by constructing a method that consists of two complementary components. High frequency errors are efficiently reduced by a *smoother*, often a traditional relaxation method, while a *coarse grid correction* that employs a hierarchy of coarser grids eliminate slow error components.

There are two ways to construct the sequence of coarse grids that are required by the coarse grid correction. In finite-difference discretisations are the dependent variables located in the grid nodes. Then *vertex-centred* coarsening is appropriate where a coarse grid is obtained by sampling the next finer grid at every other point. The *cell-centred* coarsening strategy, on the other hand, stems from finite volume discretisations which are cell based approximations of conservation laws. Here the coarse grid cells are obtained by lumping two-and-two fine grid cells in each direction, such that a two-dimensional coarse grid cell will be constructed as the union of four fine grid cells.

Traditionally the cell-centred approach was developed and applied in the field of computational fluid dynamics (see for example [1, 2] and [3] for applications to incompressible and compressible Navier-Stokes equations respectively.) Wider interest in the method was however spurred by Khalil and Wesseling [4, 5, 6] who showed that cell-centred multigrid is an attractive alternative to the vertex-centred method in problems involving discontinuous diffusion coefficients. Recently, Ersland and Teigland [7] applied cell-centred multigrid to simulation of practical reservoir problems involving discontinuous coefficients.

In this paper we discuss the performance of some traditional relaxation schemes used as smoothers in a cell-centred multigrid algorithm. First a brief description of the method is given together with convergence rates from test calculations. For the 2D Poisson equation, the line Gauss-Seidel smoother performs significantly better than the Zebra scheme, something that seems to contradict the 'conventional wisdom' that red-black patterns offer superior smoothing rates. We propose a new scheme based on red-black ordering of the coarse lines, such that lines are

*Ref. no. CMR-93-A20007. Christian Michelsen Research A/S, P.O. Box 3, N-5036 Fantoft, Norway. phone:+47-55 57 40 40, fax: +47-55 57 40 41, e-mail: thor@cmr.no

grouped two-and-two and a sequential update is made within each coarse line. This seems to be a robust parallel smoother. Finally, we perform a local mode analysis of a one-dimensional model problem in order to investigate whether the observed behaviour of the different schemes can be predicted by Fourier analysis.

2 Discretisation

In this section we will write the discrete equations for the two-dimensional Poisson equation

$$\nabla^2 \phi = f(x, y). \tag{1}$$

The equation is discretised by a finite-volume technique on a non-uniform cartesian grid. If we integrate the equation over a cell, using Gauss' theorem and approximating first derivatives with centred differences, we can write the equation for the interior cell (i, j) in stencil notation:

$$\begin{bmatrix} & a_{i,j}^{(0,+1)} & \\ a_{i,j}^{(-1,0)} & -a_{i,j}^{(0,0)} & a_{i,j}^{(+1,0)} \\ & a_{i,j}^{(0,-1)} & \end{bmatrix} \phi_{i,j} = \Delta x_i \Delta y_j f_{i,j}, \tag{2}$$

where the coefficients are

$$\begin{gathered} a_{i,j}^{(\pm 1,0)} = \frac{2\Delta y_j}{\Delta x_i + \Delta x_{i\pm 1}}, \qquad a_{i,j}^{(0,\pm 1)} = \frac{2\Delta x_i}{\Delta y_j + \Delta y_{j\pm 1}}, \\ a_{i,j}^{(0,0)} = a_{i,j}^{(+1,0)} + a_{i,j}^{(-1,0)} + a_{i,j}^{(0,+1)} + a_{i,j}^{(0,-1)}. \end{gathered} \tag{3}$$

Boundary conditions are implemented by the use of two *boundary condition masks* d and p. d has a value of unity for the Dirichlet boundary conditions and zero otherwise, while p is equal to one for the periodic boundary condition and zero otherwise. The combinations $(d, p) = (1, 0)$, $(0, 0)$ and $(0, 1)$ will then correspond to Dirichlet, Neumann and periodic boundaries respectively. The coefficients and the right hand side of the equation will be modified at the boundary:

$$\begin{gathered} a_{1,j}^{(-1,0)} = p_{0,j} \frac{2\Delta y_j}{\Delta x_{nx} + \Delta x_1}, \qquad a_{1,j}^{(0,0)} = a_{1,j}^{(+1,0)} + a_{1,j}^{(-1,0)} + a_{i,j}^{(0,+1)} + a_{i,j}^{(0,-1)} + d_{0,j} \frac{2\Delta y_j}{\Delta x_1}, \\ \Delta x_1 \Delta y_j f_{1,j} + d_{0,j} \frac{2\Delta y_j}{\Delta x_1} \phi_{0,j} + (1 - d_{0,j})(1 - p_{0,j}) \phi_{x(0,j)}, \end{gathered} \tag{4}$$

where $\phi_{0,j}$ and $\phi_{x(0,j)}$ are the Dirichlet and Neumann boundary values respectively.

3 Multigrid method

The discretised equations are solved by a linear multigrid method (correction scheme), where the correction equation

$$\boldsymbol{A} e = r, \tag{5}$$

corresponding to the discretised equation $A\phi = b$, is solved on a sequence of coarser grids. The right-hand side in (5), $r = b - \boldsymbol{A}\phi$, is called the residual.

We use cell-centred coarsening, i.e. each coarse grid cell is constructed as the union of 2^d fine grid cells, where d is the number of space dimensions. On the two-dimensional non-uniform cartesian grid, the restriction and prolongation operators are defined by area-weighted averaging and bi-linear interpolation respectively. The coarse-grid operator is discretised according to (2, 3). Because of the finite-volume discretisation, the residuals on the coarse grid can be obtained by simply adding the fine grid residuals

$$r_{\text{coarse}} = \boldsymbol{R} r_{\text{fine}} = \begin{bmatrix} 1 & 1 \\ 1 & 1 \end{bmatrix}_{\text{fine}} r_{\text{fine}}, \tag{6}$$

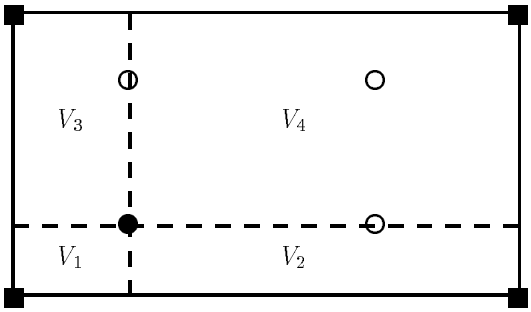

Figure 1: Interpolation volume for prolongation from the fine grid to the coarse grid.

where $\boldsymbol{R}$ is the restriction operator, and the elements in the stencil correspond to the four fine-grid points in the coarse cell. On a cartesian grid can the bilinear prolongation operator $\boldsymbol{P}$ also be interpreted as an area-weighted interpolation, where the stencil is given by:

$$\phi_{\text{fine}} = \boldsymbol{P}\phi_{\text{coarse}} = \frac{1}{V_1+V_2+V_3+V_4} \begin{bmatrix} V_2 & V_1 \\ V_4 & V_3 \end{bmatrix}_{\text{coarse}} \phi_{\text{coarse}} \tag{7}$$

where the V_i are the areas of the interpolation sub-volumes defined in figure 1. Equation 7 can also be used if it is necessary to take account of non-uniformity of the grid in the interpolation.

Gauss-Seidel type line-relaxation schemes are used as smoothers in multigrid sawtooth– and V-cycles.

4 Smoothing

Preliminary numerical experiments with different smoothers show that in some cases we can obtain significantly better convergence rates if we use the sequential line Gauss-Seidel ordering rather than the parallel Zebra ordering in the relaxation. This is contrary to what we would expect based on the smoothing factors that are found in the literature, in the 2D case the smoothing rates of Alternating Line Gauss-Seidel and Alternating Zebra are given as $\mu^{ALGS} = 0.149$ and $\mu^{AZ} = 0.048$ respectively. Model problem analysis of the Poisson equation on the unit square has shown that for a vertex-centred method, the two-grid convergence factor is directly related to the smoothing factor (Stüben and Trottenberg [8]).

In this section we present a heuristic discussion that leads to the proposal of coarse-cell red-black ordering as a parallel smoother for the cell-centred multigrid method. Finally we will give experimental convergence rates for the new scheme compared to the two other schemes in both one and two dimensions.

4.1 Coarse-cell red-black ordering

Red-black type orderings are very attractive because they offer superior smoothing rates *and* they are well suited for vector and parallel computing. The restriction and prolongation operator are both inherently parallel. Therefore, if we use a smoother with a parallel structure, we can obtain a degree of parallel efficiency in a relatively painless way. By the same argument will a sequential smoother prove a bottleneck on parallel architectures.

As we remarked above, the superior smoothing properties of the Zebra relaxation does not seem to hold for our cell-centred multigrid algorithm. As a heuristic workaround, we propose to use some other partitioning of the grid that retains a parallel structure, and at the same time can benefit, at least locally, from the serial Gauss-Seidel ordering which appears to be good for

the cell-centered approach. In the context of multigrid methods, a natural choice seems to be to perform a red-black ordering based on the coarse-grid lines, so that the two neighbouring lines that make up the coarse grid line are solved in the same sweep. We name this algorithm the *Coarse-line Zebra scheme*:

Algorithm 1 (x-Coarse-line zebra)

```
for colour = 1, 2
    for j = 5 − 2 · colour, (4), ny − 2
        solve x-line # j, j + 1
    repeat
    if j = ny − 1; solve x-line # ny − 1, ny
    else if j = ny; solve x-line # ny
    fi
repeat
```

A variant of this algorithm would be to solve the two adjacent lines that make up a coarse line simultaneously with a block-version of the tridiagonal line-solver. The results we show below are obtained by a line-by-line update within each two-line block.

4.2 Numerical experiments

As a test case, we consider the one- and two-dimensional Laplace equation with different boundary conditions on the region $\Omega = [0,1]^n,\ n = 1, 2$. As smoothers we use:

- Point Gauss-Seidel (PGS), Point Red-Black (PRB) and Coarse-Cell Red-Black (CCRB) in the 1D case.
- Alternating line Gauss-Seidel (ALGS), Alternating Zebra (AZ) and Alternating Coarse-line Zebra (ACLZ) in the 2D case.

We use line-schemes in two dimensions because they are more robust in cases when a non-uniform grid is used or with varying coefficients.

The finest grid has 64 points in each direction. The operation count is the same for all the smoothers in each case. We can therefore compare the average residual reduction factor for the multigrid iterations in order to get a measure for the efficiency of the different schemes. The average residual reduction factor, or contraction number, is:

$$\kappa = \left(\frac{\|r^n\|_2}{\|r^0\|_2} \right)^{1/n},$$

where the r^n is the residual after n iterations. In all the cases the iteration started off from random initial values and was carried out until the initial residual was reduced by a factor of 10^{-12}.

The results are given in tables 1–4. We note that, except for a few cases, the convergence is slower if we use the point/line red-black ordering compared to the lexicographic and coarse cell/line red-black orderings. The performance of the red/black and zebra relaxations also seems to depend strongly on the cycling strategy, while the results of the lexicographic and coarse cell/line red-black ordering seem to be more robust with respect to this.

Calculation of test examples involving a stretched grid show the same trends. However, if grids with rectangular cells are used, the difference between ALGS and AZ decrease for moderate to large values of the cell aspect ratio [9].

To demonstrate the possible speed-up of the method on a parallel system we performed calculations on a concurrent Alliant FX-8 with five processors. The smoother was parallelised using the appropriate compiler directives in the source code, while the rest of the program was compiled 'as is' using default optimisation options. The execution time of the program was reduced by a

Table 1: Average residual reduction. 1D, Dirichlet boundary conditions.

	V(1,0)	V(0,1)	V(1,1)
PGS	0.316	0.315	0.144
PRB	0.367	0.241	0.256
CCRB	0.291	0.279	0.108

Table 2: Average residual reduction. 2D, Dirichlet boundary conditions.

	V(1,0)	V(0,1)	V(1,1)
ALGS	0.070	0.089	0.026
AZ	0.238	0.145	0.134
ACLZ	0.134	0.128	0.058

Table 3: Average residual reduction. 2D, Neumann boundary conditions.

	V(1,0)	V(0,1)	V(1,1)
ALGS	0.145	0.086	0.025
AZ	0.211	0.133	0.108
ACLZ	0.134	0.124	0.062

Table 4: Average residual reduction. 2D, periodic boundary conditions.

	V(1,0)	V(0,1)	V(1,1)
ALGS	0.079	0.097	0.030
AZ	0.280	0.149	0.155
ACLZ	0.146	0.136	0.074

factor of approximately 2.5 when we ran the ACLZ smoother in parallel compared to scalar execution. A similar experiment using the AZ smoother showed slightly better speed-up, especially for small problems. The reason for this is probably that the parallelisation of the Zebra method gives somewhat finer granularisation and this can give better load balancing on the coarser grid levels.

5 Local mode analysis

In this section we will perform a local mode Fourier analysis of the method and the different ordering strategies for the smoother. We will first determine estimates for the smoothing rates of the different relaxation methods. A striking feature of the results of the experiments in the previous section is the relatively large discrepancy of the results for the point/line red-black orderings. In these cases we note that there is a large difference in the contraction numbers depending on whether pre- or post-smoothing is employed. In order to investigate if these effects can also be predicted by the theory, we will perform a two-level analysis of the algorithm with Gauss-Seidel and red-black ordering.

The analysis of schemes that use red-black pattern orderings is complicated by the fact that these operators do not preserve Fourier modes. The red and black steps will however be invariant in a subspace spanned by a finite number of Fourier modes. For standard red-black and zebra ordering the dimension of this subspace will be 2^d, where d is the dimension of the problem.

Stüben and Trottenberg [8] have performed a model problem analysis to determine the smoothing properties for two-colour operators, and the convergence of two-grid algorithms that use these as smoothers. Wesseling [10, 11] gives extensive results and details of a general smoothing analysis for a large number of relaxation schemes. Jay Kuo and Levy [12] analyse the red-black relaxation by expanding odd and even points in separate Fourier series. This approach has recently been used by Yavneh [13] to perform a smoothing analysis for a variety of point and block orderings applied to n-dimensional elliptical operators without cross-derivatives,

For the analysis, we will consider the one-dimensional case with point schemes on an infinite uniform grid with spacing h. We will use the cell-centred discretisation of the one-dimensional Laplace operator which has the stencil

$$u_{xx} \approx h^{-1} [1, -2, 1] u_h , \tag{8}$$

as the model equation.

5.1 Smoothing factors

We will first consider the local mode smoothing properties for the various relaxation patterns. In order to do so, we study how the relaxation method operates on the Fourier modes $\psi(\theta) =$

$\exp[-i(j-1/2)\theta]$, where $\theta = h\omega$ and ω is the frequency of the mode. For the sequential Gauss-Seidel method we then obtain the amplification factor and the smoothing rate:

$$\widehat{\boldsymbol{S}^{GS}} = e^{i\theta}/(e^{-i\theta}-2), \quad \mu^{GS} = 5^{-1/2}.$$

The red-black ordering does not preserve modes as we remarked above. We do however know that operating the red-black relaxation on the mode $\psi(\theta)$ will result in a combination of the two harmonic modes $\psi(\theta)$ and $\psi(\theta-\pi)$. For example will the first (red) half-step result in

$$\boldsymbol{S}^R = \tfrac{1}{2}\ \left[(\cos\theta+1)\psi(\theta) + i(\cos\theta-1)\psi(\theta-\pi)\right].$$

The factor i of the mode $\psi(\theta-\pi)$ comes from the translation of the grid points by half a mesh-spacing relative to the vertex-centered grid. We will see that this seemingly minor change has a profound effect on the behaviour of the scheme. If we perform a similar black half-step, we find the amplification matrix:

$$\widehat{\boldsymbol{S}^{RB}} = \frac{1}{2}\begin{pmatrix} 1+\cos\theta & -i\cos\theta(1+\cos\theta) \\ i\cos\theta(1-\cos\theta) & 1-\cos\theta \end{pmatrix}.$$

The smoothing rate corresponding to this symbol is $\mu^{RB} = 1/2$. Note that a similar analysis for a vertex-centered discretisation gives a smoothing factor of $\mu_v^{RB} = 1/8$!

To analyse the smoothing behaviour of the coarse cell red-black ordering, we write the discretised equations in the block form:

$$\boldsymbol{A}_j \begin{pmatrix} u_{2j-1} \\ u_{2j} \end{pmatrix} + \begin{pmatrix} 0 & h^{-1} \\ 0 & 0 \end{pmatrix} \begin{pmatrix} u_{2j-3} \\ u_{2j-2} \end{pmatrix} + \begin{pmatrix} 0 & 0 \\ h^{-1} & 0 \end{pmatrix} \begin{pmatrix} u_{2j+1} \\ u_{2j+2} \end{pmatrix} = \begin{pmatrix} b_{2j-1} \\ b_{2j} \end{pmatrix}, \qquad (9)$$

where $\boldsymbol{A}_j$ is the 2×2 matrix

$$\boldsymbol{A}_j = h^{-1}\begin{pmatrix} -2 & 1 \\ 1 & -2 \end{pmatrix}.$$

The block-j equation (9) can be solved exactly or approximately (by one local Gauss-Seidel iteration) at each step. Both cases can be described by a splitting of the matrix in $\boldsymbol{A}_j = \boldsymbol{M} - \boldsymbol{N}$, where we take $\boldsymbol{N} = \boldsymbol{0}$ for the exact inversion. The first half-step of the iteration can then be written:

$$\begin{pmatrix} u_{2j-1} \\ u_{2j} \end{pmatrix}^{1/2} = \begin{cases} \boldsymbol{M}^{-1}\left[\begin{pmatrix} b_{2j-1} \\ b_{2j} \end{pmatrix} + \boldsymbol{N}\begin{pmatrix} u_{2j-1} \\ u_{2j} \end{pmatrix}^{0} - h^{-1}\begin{pmatrix} u_{2j-2} \\ u_{2j+1} \end{pmatrix}^{0}\right] & j = 2k \\ \begin{pmatrix} u_{2j} \\ u_{2j+1} \end{pmatrix}^{0} & j = 2k+1 \end{cases} \qquad (10)$$

If we write a Fourier mode of the error as

$$\boldsymbol{\psi}(\theta) = \begin{pmatrix} e^{i\theta} \\ 1 \end{pmatrix} e^{i(2j-1/2)\theta}, \qquad (11)$$

then we find that the red step (10) couples the modes $\boldsymbol{\psi}(\theta)$ and $\boldsymbol{\psi}(\theta-\pi/2)$:

$$\begin{aligned} \boldsymbol{S}_R\boldsymbol{\psi}(\theta) &= \tfrac{1}{2}\ (\boldsymbol{G}+\boldsymbol{I})\begin{pmatrix} e^{i\theta} \\ 1 \end{pmatrix} e^{i2j\theta} + \tfrac{1}{2}\ (\boldsymbol{G}-\boldsymbol{I})\begin{pmatrix} e^{i\theta} \\ 1 \end{pmatrix} e^{i2j(\theta-\pi/2)} \\ &= \tfrac{1}{2}\ (\boldsymbol{G}+\boldsymbol{I})\boldsymbol{\psi}(\theta) + \tfrac{1}{2}\ (\boldsymbol{G}-\boldsymbol{I})\boldsymbol{H}\,\boldsymbol{\psi}(\theta-\pi/2) \end{aligned} \qquad (12)$$

where $\boldsymbol{I}$ is the 2×2 identity matrix, $\boldsymbol{H} = \exp(i\pi/4)\mathrm{diag}(1,i)$ and $\boldsymbol{G}$ is:

$$\boldsymbol{G}(\theta) = \boldsymbol{M}^{-1}\left[\boldsymbol{N} - h^{-1}\begin{pmatrix} e^{-i\theta} & 0 \\ 0 & e^{i\theta} \end{pmatrix}\right] \qquad (13)$$

Now, we choose $\theta \in [0, \pi/2)$, and write the error, $\boldsymbol{\varepsilon}$, in the four-dimensional subspace spanned by the Fourier modes $\boldsymbol{\psi}(\theta - l\pi/2),\ l = 0, 3$:

$$\boldsymbol{\varepsilon}_j = \sum_{l=0}^{3} c_l \boldsymbol{\psi}_l.$$

Writing the $\boldsymbol{G}$-matrices, $\boldsymbol{G}_l = \boldsymbol{G}(\theta - l\pi/2)$, we obtain the amplification matrix for the red half-step:

$$\boldsymbol{\Lambda}_R = \frac{1}{2} \begin{pmatrix} \boldsymbol{G}_0 + \boldsymbol{I} & \boldsymbol{0} & \boldsymbol{0} & (\boldsymbol{G}_3 - \boldsymbol{I})\boldsymbol{H} \\ (\boldsymbol{G}_0 - \boldsymbol{I})\boldsymbol{H} & \boldsymbol{G}_1 + \boldsymbol{I} & \boldsymbol{0} & \boldsymbol{0} \\ \boldsymbol{0} & (\boldsymbol{G}_1 - \boldsymbol{I})\boldsymbol{H} & \boldsymbol{G}_2 + \boldsymbol{I} & \boldsymbol{0} \\ \boldsymbol{0} & \boldsymbol{0} & (\boldsymbol{G}_2 - \boldsymbol{I})\boldsymbol{H} & \boldsymbol{G}_3 + \boldsymbol{I} \end{pmatrix} \tag{14}$$

The black half-step amplification matrix, $\boldsymbol{\Lambda}_B$, is found by changing the sign of the elements in the off-diagonal non-zero blocks of (14).

$$\boldsymbol{\Lambda}_B(2k+m, 2l+n) = (-1)^{k+l} \boldsymbol{\Lambda}_R(2k+m, 2l+n) \quad k, l = 0 \ldots 3 \quad m, n = 1, 2 \tag{15}$$

The smoothing factor for the method is then given by the spectral radius of the total amplification matrix, $\widehat{\boldsymbol{S}}^{CCRB} = \boldsymbol{\Lambda}_B \boldsymbol{\Lambda}_R$, projected onto the high frequency modes:

$$\mu = \rho(\boldsymbol{Q}\widehat{\boldsymbol{S}}^{CCRB}) = \max \left\{ \sup_{\theta \in [0, \pi/2)} |\lambda(\theta)| \right\}, \tag{16}$$

where $\boldsymbol{Q} = \mathrm{diag}(\boldsymbol{0}, \boldsymbol{0}, \boldsymbol{I}, \boldsymbol{I})$ is the projection operator and $\lambda(\theta)$ are the eigenvalues of $\boldsymbol{Q}\widehat{\boldsymbol{S}}^{CCRB}$. We obtain:

$$\begin{aligned} \mu^{CCRB}_{\text{exact}} &= 1/3, \\ \mu^{CCRB}_{\text{gs}} &= 3/8, \end{aligned}$$

for the algorithm with exact or approximate inversion of the 2-blocks, respectively.

Comparing the smoothing factors for the three schemes, we see that we have $\mu^{CCRB} < \mu^{GS} < \mu^{RB}$. This confirms that the trends we observed in the calculations can be qualitatively estimated by the Fourier smoothing analysis.

5.2 Two-level analysis

We will now consider the reduction of residuals and errors by the two-level algorithm given by pre-smoothing, coarse-grid correction and post-smoothing. The error iteration matrix of the two-grid algorithm is:

$$\boldsymbol{M}_e = \boldsymbol{S}_e^{\nu_2} (\boldsymbol{I}_h - \boldsymbol{P}\boldsymbol{A}_H^{-1}\boldsymbol{R}\boldsymbol{A}) \boldsymbol{S}_e^{\nu_1}, \tag{17}$$

where $\boldsymbol{S}_e$ denotes the error smoothing operator, $\boldsymbol{R}$ and $\boldsymbol{P}$ are the restriction and prolongation operators, and $\boldsymbol{A}, \boldsymbol{A}_H$ are the discrete equations on the fine and coarse grid. $\nu_{1,2}$ is the number of pre- and post-smoothing sweeps respectively. Similarly, we have the residual iteration matrix

$$\boldsymbol{M}_r = \boldsymbol{S}_r^{\nu_2} (\boldsymbol{I}_h - \boldsymbol{A}\boldsymbol{P}\boldsymbol{A}_H^{-1}\boldsymbol{R}) \boldsymbol{S}_r^{\nu_1}, \tag{18}$$

where the residual smoothing operator is $\boldsymbol{S}_r = \boldsymbol{A}\boldsymbol{S}_e\boldsymbol{A}^{-1}$.

To facilitate the analysis of the transfer operators, we introduce the elementary restriction and prolongation operators. The elementary restriction is an injection-like operator that is defined for cell-centred coarsening by

$$(\boldsymbol{R}^0 u_h)((j - \tfrac{1}{2})2h) = u_h((2j - \tfrac{1}{2})h), \tag{19}$$

and the elementary prolongation is:

$$(\boldsymbol{P}^0 u_{2h})((j-\tfrac{1}{2})h) = \begin{cases} u_{2h}((k-\frac{1}{2})2h), & j=2k \\ 0, & j=2k+1 \end{cases} \tag{20}$$

The one-dimensional cell-centred averaging and interpolation operators corresponding to eqs. (6, 7) can then conveniently be written as a combination of these operators and a grid function acting on the fine grid.

$$\boldsymbol{R} = \boldsymbol{R}^0[1,1,0]_h, \tag{21}$$

$$\boldsymbol{P} = [\tfrac{1}{4},\tfrac{3}{4},\tfrac{3}{4},\tfrac{1}{4},0]_h\,\boldsymbol{P}^\circ. \tag{22}$$

To find the Fourier representations of the different operators and the two-grid amplification matrix, we define the Fourier transform of a discrete function, $u_h \in L_h^2$, on the cell-centred grid:

$$\widehat{u_h} = \frac{h}{\sqrt{2\pi}} \sum_j e^{-i(j-1/2)h\omega} u_h((j-1/2)h), \tag{23}$$

where the frequency can be represented on the h-grid: $\omega \in T_h = [-\pi/h, \pi/h)$.

The matrices corresponding to the discretised equations, $\boldsymbol{A} and \boldsymbol{A}_H$, are both Toeplitz operators, that is they have both constant stencils, with Fourier symbols:

$$\widehat{\boldsymbol{A}}(\theta) = -\frac{4\sin^2\theta/2}{h}, \quad \widehat{\boldsymbol{A}_H}(\theta) = -\frac{2\sin^2\theta}{h}, \quad \theta = h\omega. \tag{24}$$

Using equations (19,20,23), we obtain the Fourier transforms of the elementary transfer operators (cf. Hemker [14], Molenaar [15]):

$$\widehat{R^0 u_h}(\theta) = e^{i\theta/2} \sum_{p=0,1} e^{-ip\pi/2} \widehat{u_h}(\theta - p\pi), \tag{25}$$

$$\widehat{P^0 u_{2h}}(\theta - p\pi) = \tfrac{1}{2}\, e^{-i(\theta-p\pi)/2} \widehat{u_{2h}}(\theta). \tag{26}$$

Equation (25) shows that the restriction operation aliases high and low frequencies. In both of the above equations, we therefore have $\theta \in hT_{2h} = [-\pi/2, \pi/2)$. Because of the aliasing, we will write the Fourier transform of a u_h-grid-function as a vector with components from the harmonic modes $(\theta, \theta-\pi)$ where $\theta \in hT_{2h}$. From equations (21) and (25), we find that the Fourier transform of the restriction can be written as the 1×2 matrix:

$$\widehat{R}(\theta) = 2(\cos\theta/2, \sin\theta/2). \tag{27}$$

Similarly, we obtain the symbol for the prolongation written as the 2×1 vector

$$\widehat{P}(\theta) = \frac{e^{-i\theta}}{4} \begin{pmatrix} \cos 3\theta/2 + 3\cos\theta/2 \\ \sin 3\theta/2 - 3\sin\theta/2 \end{pmatrix}. \tag{28}$$

Combining these results with the symbols of the relaxation operators, the two-level amplification matrices are obtained for sequential and red-black smoothing. We consider the spectral radius and the spectral norm of the two-grid operator $\widehat{\boldsymbol{M}}$,

$$\rho(\widehat{\boldsymbol{M}}) = \max\left\{ \sup_{\theta \in hT_{2h}} |\lambda(\theta)| \right\}$$

$$\|\widehat{\boldsymbol{M}}\|_s = \sqrt{\rho(\widehat{\boldsymbol{M}}^H \widehat{\boldsymbol{M}})}.$$

By evaluating the eigenvalues of the two-level amplification matrix, we find $\rho(M_e) = \rho(M_r)$. The spectral radii are given in Table 5. In all the cases are the spectral radii bounded below

Table 5: Spectral radius of the residual amplification matrix for the two-grid algorithm.

	2G(1,0)	2G(0,1)	2G(1,1)
PGS	0.48	0.48	0.35
PRB	0.59	0.59	0.39

Table 6: Spectral norm of the residual amplification matrix for the two-grid algorithm.

	2G(1,0)	2G(0,1)	2G(1,1)
PGS	0.70	0.70	0.36
PRB	0.80	1.00	0.44

unity so that the convergence of the method is assured. In some cases the spectral norm of the error amplification matrix becomes unbounded when $\theta = 0$ and this indicates that some error components may be blown up in the first iterations. In practice will however the $\theta = 0$-mode be excluded from the error by boundary conditions or a global constraint on the solution. The norms of the residual iteration matrices are all bounded (Table 6), and we note that this norm is somewhat larger for the (1,0)-cycle than for the (0,1)-cycle. Thus may the difference we noticed between these cycles in the numerical experiments indeed be predicted, at least in part, by this analysis.

6 Conclusions

By a local mode analysis we have shown that the proposed coarse cell red-black ordering is indeed an efficient smoother for the cell-centred multigrid algorithm. The translation of the grid points relative to the vertex-centred grid changes the Fourier symbol of the standard red-black ordering and, as a consequence, the smoothing rate of this scheme deteriorates in the cell-centred algorithm. The results of the two-level analysis is not conclusive, but the norms of the two-grid operator confirm that Gauss-Seidel relaxation is a more efficient smoother than the red-black scheme for cell-centred multigrid. Furthermore, the spectral norm of the residual amplification matrix can indicate that post-smoothing is more efficient than pre-smoothing when we use the red-black relaxation as a smoother. Thus do the results of the analysis agree qualitatively with the observed behaviour of the algorithm. However, in all the cases does the prediction of the analysis overestimate the convergence factors of the method.

Acknowledgements

I thank professors Carlo Benocci and Herman Deconinck for their help during the first part of this work. Furthermore, professor Pieter W. Hemker for excellent advice and for pointing out the way forward at a crucial time, and my colleague Dr. Rune Teigland for valuable suggestions and discussions.

This work was supported by the Research Council of Norway through grants no. ST.30.100.221747 (NATO Science Fellowship) and ST.10.12.222076.

References

[1] S. P. Vanka. Block-implicit multigrid solution of navier-stokes equations in primitive variables. *Journal of Computational Physics*, 65:138–158, 1985.

[2] C. Becker, J. H. Ferziger, M. Perić, and G. Scheurer. Finite volume multigrid solutions of the two-dimensional incompressible Navier-Stokes equations. *Notes on Numerical Fluid Mechanics*, 23:37–47, 1988.

[3] B. Koren. *Multigrid and defect correction for the steady Navier-Stokes equations, application to aerodynamics*, volume 74 of *CWI Tracts*. CWI, Amsterdam, 1991.

[4] P. Wesseling. Cell-centered multigrid for interface problems. In S. F. McCormick, editor, *Multigrid Methods: Theory, applications, and supercomputing.*, volume 110 of *Lecture Notes in Pure and Applied Mathematics*, pages 631–641. Marcel Dekker Inc., 1988.

[5] M. Khalil. *Analysis of Linear Multigrid Methods for Elliptic Differential Equations with Discontinuous and Anisotropic Coefficients*. Ph.D. thesis, Delft University of Technology, 1989.

[6] M. Khalil and P. Wesseling. Vertex-centered and cell-centered multigrid for interface problems. *Journal of Computational Physics*, 98:1–10, 1992.

[7] B. G. Ersland and R. Teigland. Comparison of two cell-centered multigrid schemes for problems with discontinuous coefficients. *Numerical Methods for Partial Differential Equations*, 9:265–283, 1993.

[8] K. Stüben and U. Trottenberg. Multigrid methods: Fundamental algorithms, model problem analysis and applications. In W. Hackbusch and U. Trottenberg, editors, *Multigrid Methods*, number 960 in Lecture Notes in Mathematics, pages 1 – 176. Springer Verlag, 1982.

[9] T. Gjesdal. Development of a multigrid method for the pressure Poisson equation. Project Report PR 1992-18, von Karman Institute for Fluid Dynamics, Rhode Saint Genese, Belgium, 1992.

[10] P. Wesseling. A survey of Fourier smoothing analysis results. In W. Hackbusch and U. Trottenberg, editors, *Multigrid Methods III*, volume 98 of *International Series of Numerical Mathematics*, pages 105–127. Birkhäuser Verlag Basel, 1991.

[11] P. Wesseling. *An Introduction to Multigrid Methods*. Pure and Applied Mathematics. John Wiley & Sons, 1992.

[12] C.-C. Jay Kuo and B. C. Levy. Two-color Fourier analysis of the multigrid method with Red-Black Gauss-Seidel smoothing. *Applied Mathematics and Computation*, 29:69–87, 1989.

[13] I. Yavneh. Multigrid smoothing factors for red-black Gauss-Seidel applied to a class of elliptic operators. Submitted to *SIAM J. Num. Anal.* A preprint of the paper is available by anonymous ftp from `casper.cs.yale.edu` in the subdirectory `mgnet/papers/Yavneh`, 1993.

[14] P. W. Hemker. Fourier analysis of gridfunctions, prolongations and restrictions. Report NW 93/80, Dept. of Numerical Mathematics, Mathematical Center, Amsterdam, 1980.

[15] J. Molenaar. A two-grid analysis of the combination of mixed finite elements and Vanka-type relaxation. In W. Hackbusch and U. Trottenberg, editors, *Multigrid Methods III*, volume 98 of *International Series of Numerical Mathematics*, pages 313–324, Basel, 1991. Birkhäuser.